Radiation-Induced Decomposition of PETN and TATB under Extreme Conditions

Hubertus Giefers* and Michael Pravica

High Pressure Science and Engineering Center (HiPSEC), Department of Physics and Astronomy, University of Nevada Las Vegas, Las Vegas, Nevada 89154-4002

Received: October 31, 2007; In Final Form: January 13, 2008

We conducted a series of experiments investigating decomposition of secondary explosives PETN and TATB at varying static pressures and temperatures using synchrotron radiation. As seen in our earlier work, the decomposition rate of TATB at ambient temperature slows systematically with increasing pressure up to at least 26 GPa but varies little with pressure in PETN at ambient temperature up to 15.7 GPa, yielding important information pertaining to the activation complex volume in both cases. We also investigated the radiation-induced decomposition rate as a function of temperature at ambient pressure and 26 GPa for TATB up to 403 K, observing that the decomposition rate increases with increasing temperature as expected. The activation energy for the TATB reaction at ambient temperature was experimentally determined to be 16 ± 3 kJ/mol.

Introduction

The mechanism of detonation of explosives at the molecular level remains a yet unsolved problem in chemical physics. How mechanical energy from a shock wave is transferred into localized bonds of energetic molecules to initiate chemical reactions is not well understood.[1] Precisely which bonds absorb this energy and cause molecular decomposition is also of much interest. Some of the inherent difficulties associated with detonation studies lie in the rapid progress of the shockwave initiating and consuming the explosive, which is usually on the order of hundreds of nanoseconds, making dynamic measurements difficult. One alternative and complementary approach to understand reaction processes at the molecular level is to simulate and study how static application of high pressure and high temperature (as would be experienced in a shockwave) affect the unreacted energetic materials. Observation can proceed on a much longer time scale. Considerable effort has been expended in this area using diamond anvil cells.[1−6]

As explosives are utilized for a wide variety of applications, which can include the initiation of nuclear fission, it would also be of great interest to better understand their behavior when subjected to high- or even low-level (when in storage) ionizing radiation flux. Recent antiterrorist efforts to detect bombs (including "dirty" bombs) using X-ray scanners[7−8] provoke questions relating to the sensitization (or desensitization) of explosives by ionizing radiation.

There have also been concerns where organic compounds were formed over time from solvents used to clean radioactive waste and might detonate via ionizing radiation from the waste.[9−10] Finally, ionization is another method that adds energy to a molecular system via bond rearrangements. It may yield useful insights into how the electronic structure of these complex molecules alters, leading to a chemical reaction without adding random macroscopic thermal energy to complicate the data.

Some past studies have used proton and electron beams[11−14] and other ionizing rays[15−18] including X-rays[19−20] to neutralize, desensitize, or detonate explosives. However, with the exception of studies in refs 1 and 5, none of these studies were performed at pressures beyond ambient, and of these two studies, none have systematically studied radiation-induced damage at elevated pressure. Yet pressure is an important thermodynamic variable that can yield much information not only on the survivability and transformations of energetic materials but also about the chemistry causing these transformations (e.g., the activation volume).

In the interest of contributing to the understanding of these vital materials, we have undertaken a series of studies aimed at discerning the behavior of energetic materials under extreme conditions of pressure, temperature, and ionizing radiation.

This paper represents a continuation of our efforts to better understand the behavior of useful secondary energetic materials under extreme conditions of pressure,[21−24] high radiation flux,[25]

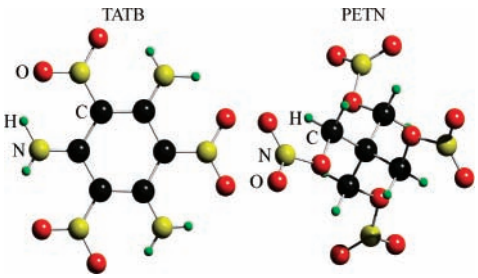

Figure 1. Ball-and-stick model for (left) TATB and (right) PETN.

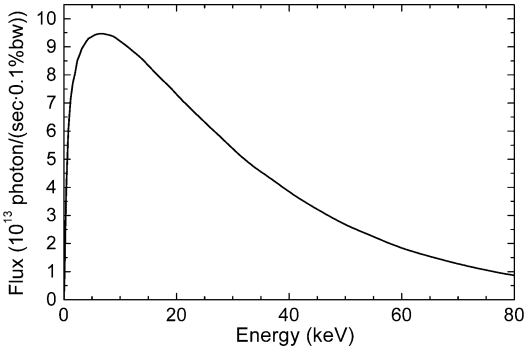

Figure 2. Theoretically calculated spectrum from the APS synchrotron as delivered to the experimental hutch.

* To whom correspondence should be addressed. Phone: 702-895-1718. Fax: 702-895-0804. E-mail: hubertus@physics.unlv.edu.

10.1021/jp710512b CCC: $40.75 © 2008 American Chemical Society
Published on Web 03/12/2008

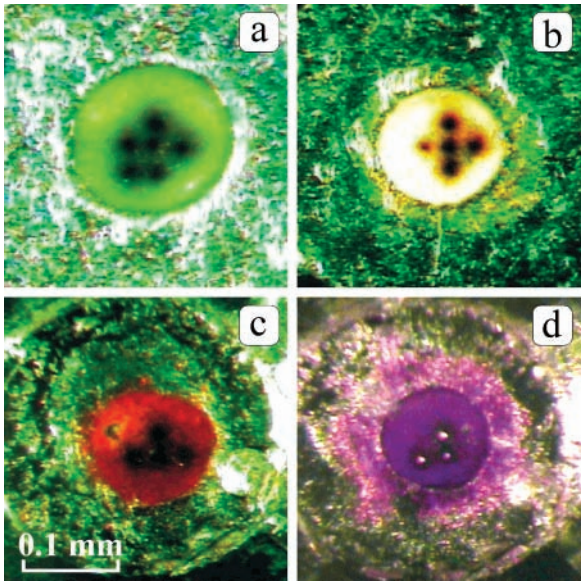

Figure 3. Photographs of the sample environment in the DAC after in situ experiments with TATB: (a) at ambient conditions, (b) 5.3 GPa, (c) 17.0 GPa, and (d) 26.6 GPa. The sample was illuminated from above. The greenish appearance of the gasket is an artifact of the microscope lighting. The actual gasket appearance is bluish gray.

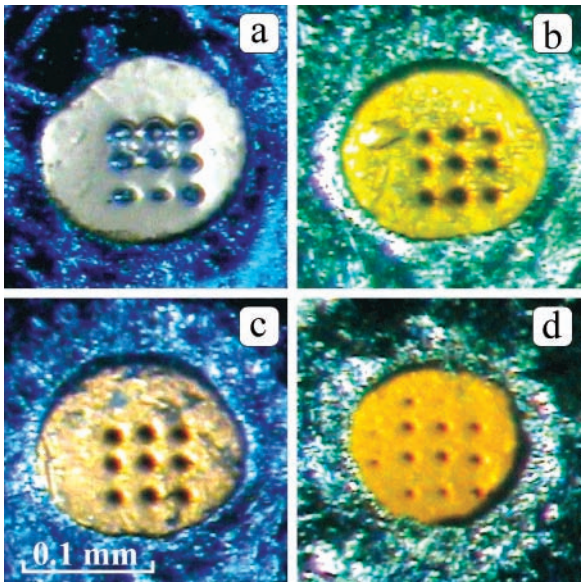

Figure 4. Photographs of the sample environment in the DAC after in situ experiments with PETN: (a) at ambient conditions, (b) 5.9 GPa, (c) 10.9 GPa, and (d) 15.7 GPa. Photos were taken with light shining through the sample.

temperature, and any combination thereof.[26] We performed three sets of white-beam, energy-dispersive diffraction experiments on PETN (pentaerythritol tetranitrate) and TATB (1,3,5-triamino-2,4,6-trinitrobenzene) (see Figure 1). We observed the time dependence of the integrated, background-subtracted intensities of visible diffraction lines to determine radiation-induced decomposition rates as functions of pressure (PETN and TATB) and temperature (TATB). From the data garnered, important chemical reaction parameters were determined. Some of these constants such as the sign of the activation volume are difficult to determine otherwise.[27]

Experimental Section

White PETN and yellow TATB submicrometer powder was placed in a Mao-Bell-type diamond anvil cell (DAC)[28] using

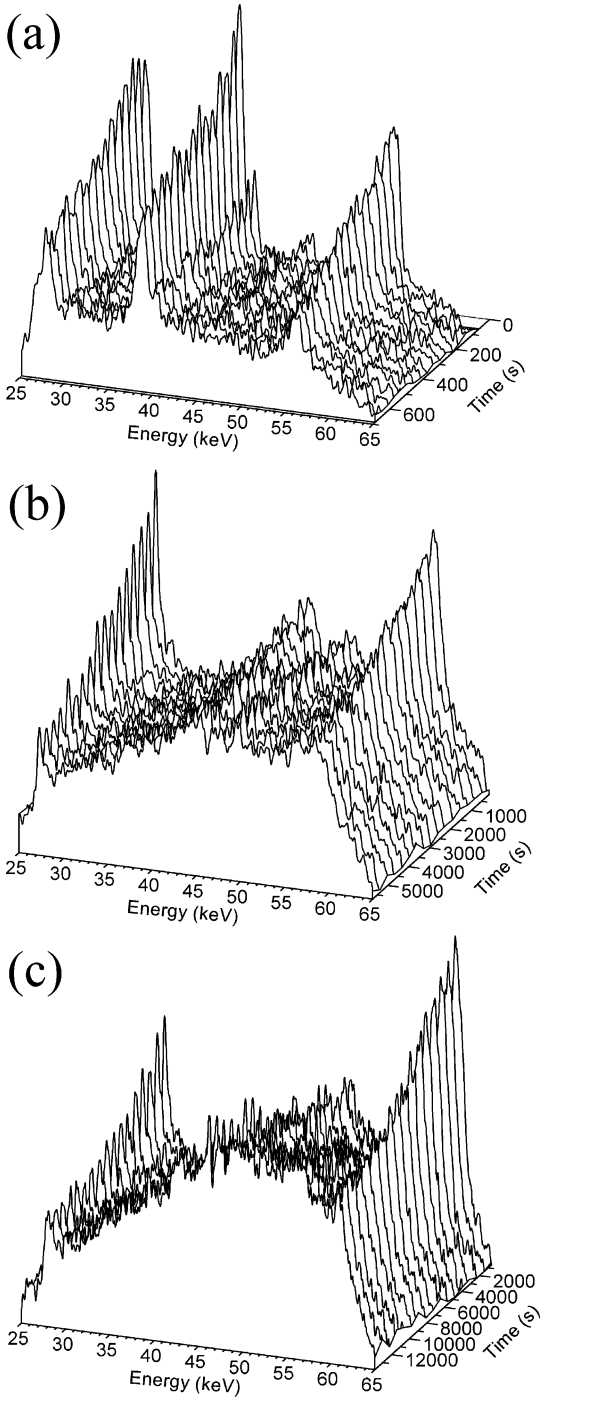

Figure 5. Energy-dispersive X-ray diffraction patterns of the in situ decompositions of TATB at (a) ambient conditions, (b) 10.8 GPa, and (c) 26.6 GPa. The counting times were (a) 40, (b) 270, and (c) 420 s for each spectrum.

400 and 300 μm culets in separate experiments described below. As TATB slowly alters with time in the presence of UV light, turning greenish yellow, we were especially careful to load the TATB samples quickly and with as little light as possible during the loading process until confined by the diamonds and gasket. The gaskets in the experiments were made of Re and preindented to ~40−80 μm initial thickness (depending on the ultimate pressure desired). The gasket holes were drilled via electric discharge machining and were ~100−150 μm in diameter. No pressure medium was used in our experiments. Variation of pressure within the sample is typically less than 5% of the measured pressure. Thermally treated, strain-relieved ruby spheres were used to measure the sample pressure.[29] An external

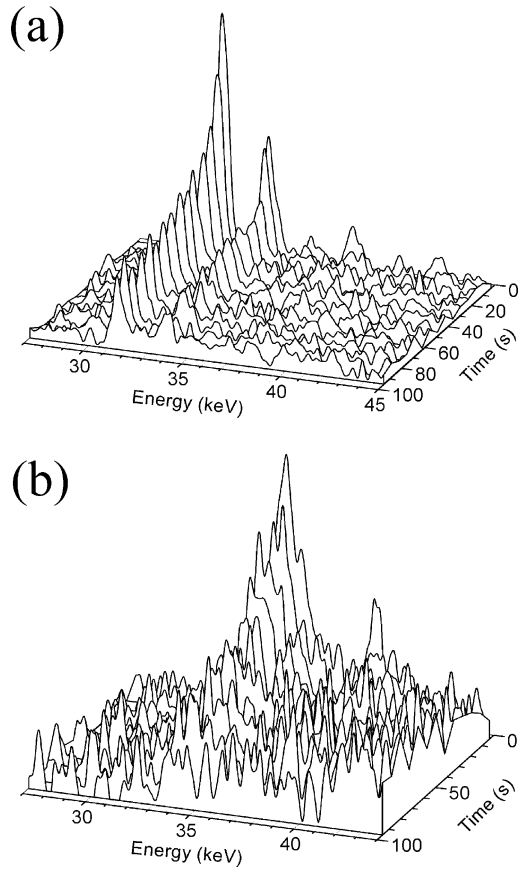

Figure 6. Energy-dispersive X-ray diffraction patterns of the in situ decompositions of PETN at ambient conditions and 15.7 GPa. The counting times were (a) 5 and (b) 7 s for each spectrum.

resistive heater was used to increase the temperature of the DAC for the kinetic experiments at elevated temperatures. Temperature was measured using a thermocouple close to the sample. At the highest temperature in the experiments (403 K), it took about 2 h to stabilize the temperature expansion of the entire set up within the size of the synchrotron beam. Our experiments were performed at the High-Pressure Collaborative Access Team's (HP-CAT's) energy-dispersive X-ray diffraction beamline, 16 BM-D, using white synchrotron radiation from a bending magnet at the APS storage ring. A theoretical X-ray energy spectrum curve of the synchrotron radiation delivered into our experimental hutch is displayed in Figure 2. The white X-ray beam was focused to a spot size of about 5 μm FWHM using Rh-coated Kirkpatrick-Baez mirrors. Energy-dispersed X-ray diffraction (EDXRD) patterns were collected within a diffraction angle, $2\Theta_B$, of 6.00° and analyzed using Origin.

Due to the small 5 μm focused beam size and the large sample chamber, several kinetic runs could be performed with each sample preparation. The experimental runs are separated by 25 μm within the sample. Each run left a noticeable mark in the sample as shown in Figures 3 and 4. Nine or more runs were performed when the reaction kinetics was fast, and fewer runs were conducted when the reaction progressed slowly.

For the first experiment, PETN powder was compressed up to 15.7 GPa using a diamond anvil cell at ambient temperature and the radiation-induced decomposition rate was measured as a function of pressure. In the second experiment, TATB powder was compressed up to 26.6 GPa at ambient temperature and the radiation-induced decomposition rate was measured as a function of pressure. Finally, in the third experiment, TATB powder was heated at ambient pressure and 26 GPa and the decomposition rate was measured as a function of temperature up to 403 K. Throughout the experiments, we found little evidence of global sample heating measuring less than 2 K change with a thermocouple placed near the sample. Thus, we effectively focus our work on one involving pressure/volume and possibly electronic activation via bond rearrangements/ionization by removing complications due to global sample heating/vibrational excitation. With a focused beam, we found that the explosive in the beam rapidly discolored over times that coincided with a loss of diffraction intensity in the region we observed. By moving our sample (which was much larger than our beam spot size) relative to the X-ray beam, we could repeat the experiment multiple times.

As seen in our earlier studies,[26] PETN decomposes rapidly. To reduce this reaction rate, we reduced the X-ray flux at the sample by placing two photon absorbers (700 μm Al and 100 μm Cu) in front of the DAC at ambient conditions and the highest pressure.

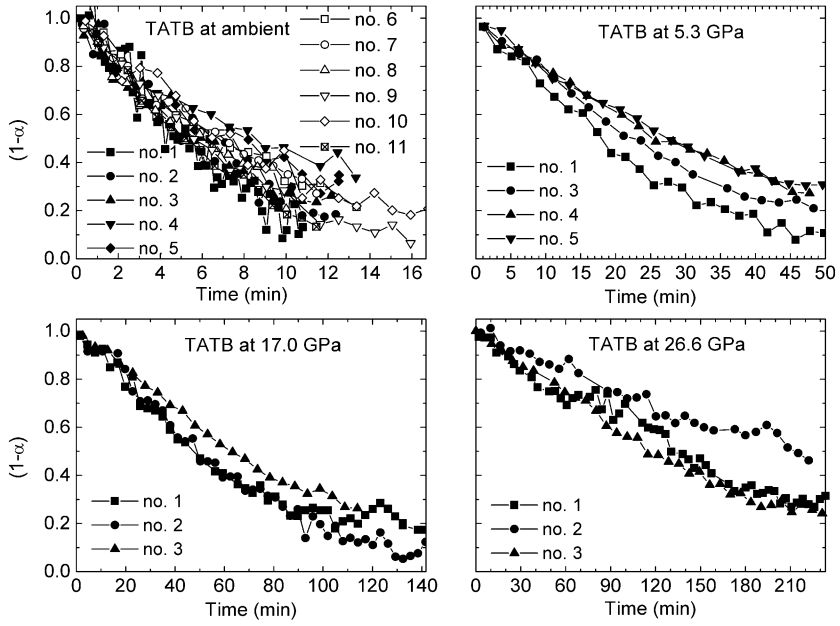

Figure 7. Progress of the radiation-induced decompositions of TATB.

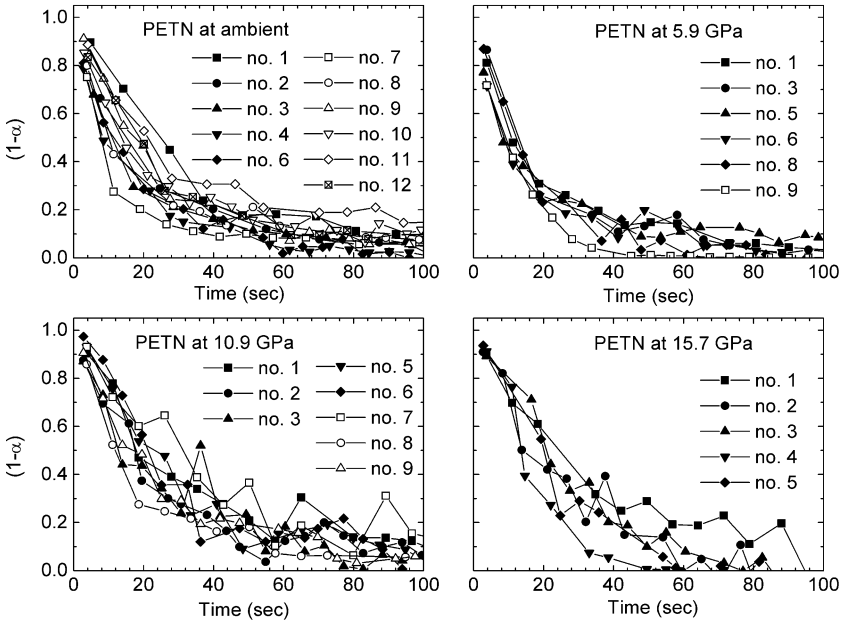

Figure 8. Progress of the radiation-induced decompositions of PETN.

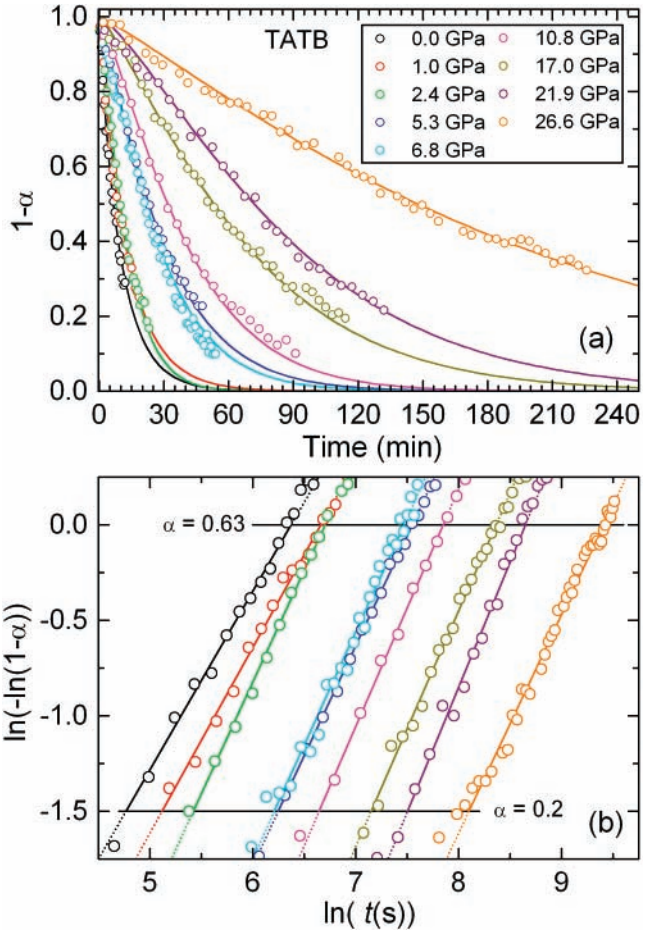

Figure 9. (a) Comparison of the progress of the radiation-induced decomposition of TATB at ambient temperature. The data are combinations of several runs shown in part in Figure 7. The continuous lines are the fitted function (see Figure 9b). (b) Sharp−Hancock plot of the radiation-induced reaction progress α for TATB. The horizontal lines give the interval for fitting the data.

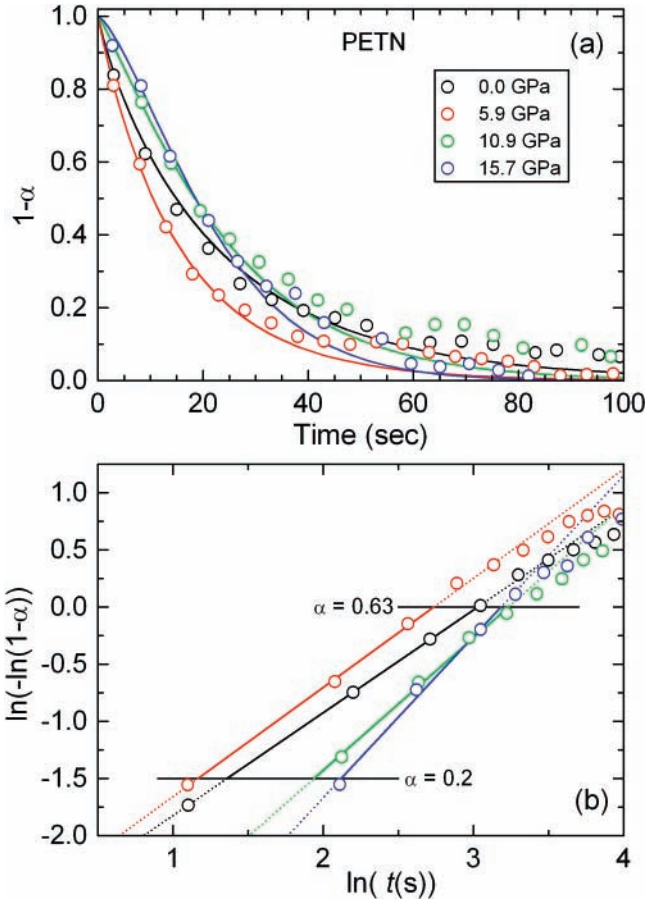

Figure 10. Radiation-induced decomposition of PETN at different pressures at ambient temperature. The two graphs are explained in the caption of Figure 9.

In Figure 3, a color change of the TATB sample is evident with pressure. The color alters with pressure up to about 12 GPa from yellow → green → red. Beyond this pressure, the color becomes intensely red and at about 24 GPa opaque and black. The violet color in Figure 3d is miscolored due to illumination from the microscope viewing optics. The color changes back to yellow-green with minor reddish spots after pressure release, even when pressurized as high as 31 GPa. From prior studies[23] we know that TATB survives pressure cycling to at least 10 GPa at ambient temperature. The synchrotron radiation changes the color of the sample TATB to black. Due

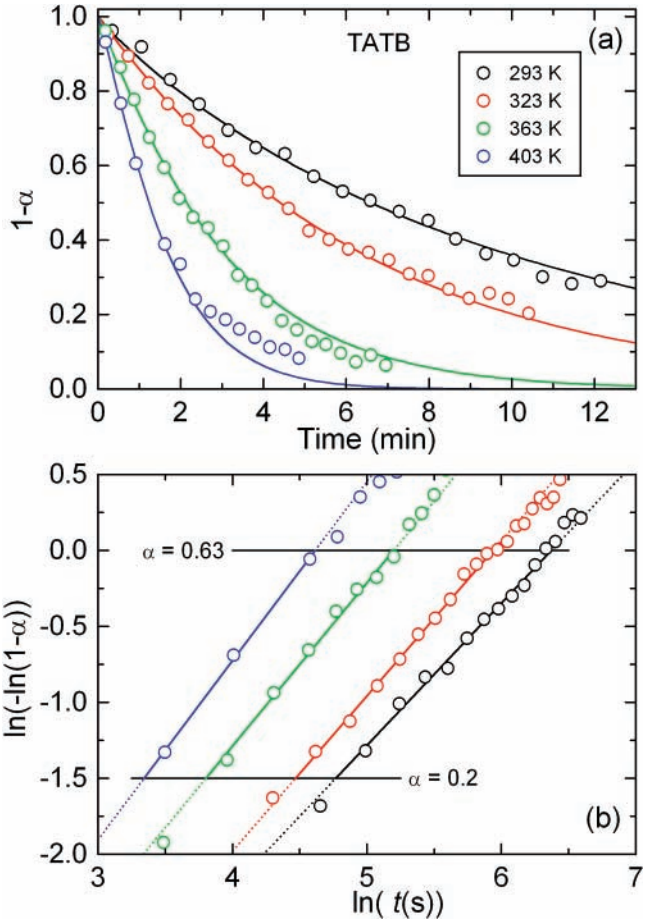

Figure 11. Radiation-induced decomposition of TATB at different temperatures at ambient pressure. The two graphs are explained in the caption of Figure 9.

TABLE 1: Reaction Parameters for the Radiation-Induced Decomposition in TATB and PETN

sample	p (GPa)	T (K)	m	ln k (s^{-1})	$t_{0.5}$ (s)	additional material in SR beam
TATB	0.0	293	0.9	−6.37	395	
TATB	0.0	323	1.0	−5.65	199	
TATB	0.0	363	1.1	−5.20	129	
TATB	0.0	403	1.2	−4.62	74	
TATB	1.0	293	1.0	−6.66	536	
TATB	2.4	293	1.2	−6.70	596	
TATB	5.3	293	1.2	−7.55	1383	
TATB	6.8	293	1.2	−7.47	1289	
TATB	10.8	293	1.2	−7.85	1909	
TATB	17.0	293	1.2	−8.37	3192	
TATB	21.9	293	1.3	−8.65	4310	
TATB	26.6	293	1.1	−9.41	8860	
TATB	25.2	403	1.2	−8.25	2842	
PETN	0.0	293	0.9	−3.03	14	
PETN	0.0	293	0.9	−3.54	23	700 μm Al
PETN	0.0	293	0.8	−4.69	69	100 μm Cu
PETN	5.9	293	1.0	−2.74	11	
PETN	10.9	293	1.2	−3.23	18	
PETN	15.7	293	1.4	−3.18	19	
PETN	15.7	293	0.6	−4.21	38	700 μm Al
PETN	15.7	293	0.9	−5.16	118	100 μm Cu

to the Lorentzian shape of the intensity distribution across the beam, a much larger spot than 5 μm in diameter becomes black (Figure 3) but it is still far smaller than the sample diameter. At the highest pressure in the experiments of 26.6 GPa and a synchrotron bombardment of about 4 h, the black color of the TATB reaction products alters to become transparent in the tiny region of the highest radiation flux (Figure 3d).

The transparent PETN sample remained so at the highest pressure in our experiments (~16 GPa). The reaction products which appear red under pressure (Figure 4b−d) become gaseous at ambient conditions (Figure 4a).

In both cases, we were unable to determine the reaction products.

Results

For each run, 15−50 diffraction patterns were collected and evaluated to ascertain the progress of the reaction. The counting time per spectrum was between 5 and 15 s for PETN and 20 and 420 s for TATB. The diffraction patterns were continuously recorded during each run at one damage spot in the sample. The time evolution of diffraction patterns of some runs are shown in Figures 5 and 6.

Background-subtracted intensities of characteristic diffraction lines were used to evaluate the rate of decomposition of the energetic materials subject to the X-ray beam. For PETN, the strongest observed diffraction line (201) was used to reference decomposition. For TATB, the strongest observed diffraction lines (−421, −2−22, 2−40, 2−42, 220, 4−21) in the 55−60 keV energy range were used. The strongest diffraction line of TATB (002) at 37.5 keV at ambient pressure overlaps with a newly emerging diffraction line at about 37.0 keV, which grows during the decomposition reaction. Because both lines overlap strongly, neither the TATB (002) nor the new diffraction line could be used to evaluate the data further. The relatively rapid decomposition of PETN and TATB precluded measuring an EDXRD pattern at $t = 0$ for normalization. The normalization factors for converting intensity into virgin sample concentration were determined by fitting a 3−5 order polynomial function to the intensity vs time values and extracting the normalization value/initial intensity at $t = 0$. The normalization values were determined for each run separately, and the integrated intensity values were subsequently divided by the evaluated normalization values to extract the unreacted concentration of the explosive with time. Due to the decreasing synchrotron intensity with time, the slowing of the kinetics was compensated by shrinking the time axis. All spectra were normalized to a 102 mA synchrotron beam intensity current in the storage ring. Some time-dependent concentrations for several runs are shown in Figures 7 and 8. The time scales in the case of TATB are very different. The several data sets of unreacted concentrations versus time for each pressure/temperature value were added together and divided by the number of runs to extract the mean concentration versus time curves shown in Figures 9a−11a.

The time-dependent concentrations of the unreacted energetic material (Figures 9a−11a), $(1 - \alpha)$, with α $(0 \le \alpha \le 1)$ representing the reaction progress, were evaluated by implementing Avrami−Erofeyev kinetics

$$\alpha = 1 - \exp(-(kt)^m) \quad (1)$$

by using the linearized form

$$\ln(-\ln(1 - \alpha)) = m \cdot \ln(k) + m \cdot \ln(t) \quad (2)$$

We used the Sharp−Hancock plot,[30−31] $\ln(-\ln(1 - \alpha))$ vs $\ln(t)$, to obtain the reaction exponent m, which is an important indicator of the rate-determining reaction step, and also the reaction rate constant k. The reaction exponent m is the slope, and $m \cdot \ln(k)$ is the intercept with the ordinate in the Sharp−Hancock plot for the interval $\alpha = 0.2-0.63$ (see Table 3 of ref 32). The time progressions for the runs from Figures 9a−11a are shown as Sharp−Hancock plots in Figures 9b−11b,

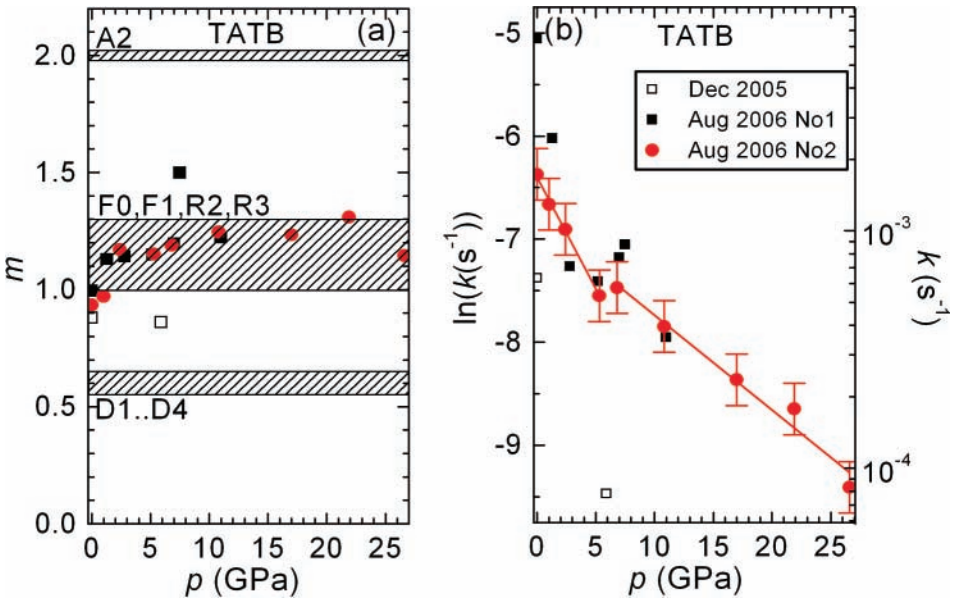

Figure 12. (a) Reaction exponent, *m* (left), and (b) rate coefficient, *k* (right), for the radiation-induced decomposition of TATB at different pressures at ambient temperature. The abbreviations refer to the rate equations listed in Table 3 of ref 25.

respectively. The Sharp−Hancock plots show that in this graphical representation the different reaction curves are almost parallel. This implies that the reaction mechanism is independent of pressure, temperature, and even energetic material when comparing the values of *m*.

The characteristic times, $t_{0.5}$, wherein one-half of the starting material has reacted, can be calculated using

$$t_{0.5} = \frac{(\ln 2)^{1/m}}{k} \tag{3}$$

The values for *m*, ln *k*, and $t_{0.5}$ under all of the different experimental conditions for PETN and TATB are listed in Table 1.

The reaction parameters for TATB at high pressure and ambient temperature are plotted in Figure 12 together with results from former experiments with different synchrotron beam characteristics such as beam size and energy spectrum. The reaction exponent is very similar for all of the experiments and varies between 0.9 and 1.3. However, the reaction rate constant *k* shows pronounced pressure dependence. With increasing pressure, the reaction rate consistently slows with pressure and is lowest at the highest pressure of 26.6 GPa. Compared to the Aug 2006 No1 runs, the slope of *k* at low pressure (to a pressure of 5 GPa) of the Aug 2006 No2 runs is less negative (Figure 12b). The trend of *k* can be split into two intervals with a linear behavior: the first one from 0 to 5.3 GPa, and the second one from 6.8 to 26.6 GPa. The pressure dependence of the reaction rate constant, d(ln *k*)/d*p*, of TATB between 0 and 5.3 GPa is $-0.22(5)$ GPa^{-1}, and between 6.8 and 26.6 GPa, this value is $-0.092(10)$ GPa^{-1}. These results qualitatively agree with Satija's observation that photolysis of TATB slows above 1.5 GPa,[1] suggesting a positive activation volume.[1] The slow decomposition of TATB at ambient pressure and ambient temperature was also qualitatively seen by Sharma[20] though Sharma was using Mg K lines for X-ray photoelectron spectroscopy excitation, whereas we used full spectrum synchrotron radiation for our damage studies.

As shown in refs 2 (eq 14) and 26 transition-state theory yields, with some assumptions, the equation

$$\left(\frac{\partial \ln k}{\partial p}\right)_T = \frac{-\Delta V^{\ddagger}}{RT} \tag{4}$$

with $\Delta V^{\ddagger}$ being the volume of activation, $R = 8.3145$ J/(K·mol) the universal gas constant, and *T* the absolute temperature. $\Delta V^{\ddagger}$ is volume difference between the transition state and reactant. With eq 4 and the pressure dependence of *k*, we calculate the activation volume between 0 and 5.3 GPa to be $\Delta V^{\ddagger} = 0.54(13)$ cm^3/mol and between 6.8 and 26.6 GPa to be $\Delta V^{\ddagger} = 0.22(3)$ cm^3/mol, i.e., TATB shows the expected behavior of a decreasing $|\Delta V^{\ddagger}|$ with increasing pressure.

Here, we should state that we get very different results at low pressure if the data of the Aug 2006 No 1 runs are considered (see Figure 11). The experimental conditions were similar, and the same sample was used as in the runs of the Aug 2006 No2 experiments. The pressure dependence of *k* between 0 and 2.8 GPa leads to an activation volume of $\Delta V^{\ddagger} = 1.9$ cm^3/mol, which is about 3.5 times larger than in the Aug 2006 No2 experiments. The origin for these different results at low pressure is unknown.

The reaction exponent *m* and the reaction rate constant *k* of PETN with pressure are shown in Figure 13. The reaction exponent *m* is difficult to determine in our experiments in the very fast reaction of PETN, where only 3−4 data points (Figure 10b) are available in the range $\alpha = 0.2-0.62$. Nevertheless, the reaction exponent *m* is about 1 ± 0.4 within the pressure range to about 16 GPa and with different synchrotron beam characteristics. The reaction rate *k* is constant within the error bars to 16 GPa, as earlier observed in a lower pressure range,[26] and an activation volume, which is close to zero, cannot be determined with these experiments. The experiments, where different radiation absorbers were placed in the synchrotron beam, verify these findings to within the experimental errors. The value for *k* at ambient conditions and without radiation absorbers confirm the result found in the experiments of the Aug 2006 No1 runs, which in turn shows that similar conditions were used in both Aug 2006 runs.

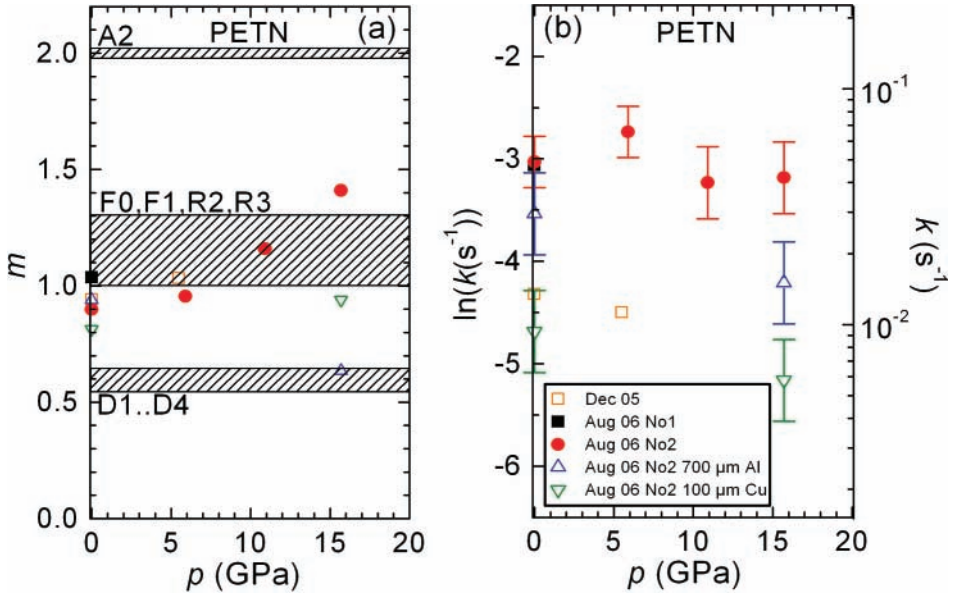

Figure 13. (a) Reaction exponent, *m* (left), and (b) rate coefficient, *k* (right), for the radiation-induced decomposition of PETN at different pressures at ambient temperature. The abbreviations refer to the rate equations listed in Table 3 of ref 25.

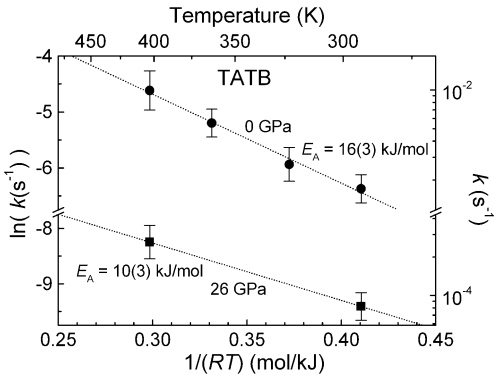

Figure 14. Arrhenius plot ln(*k*) vs 1/*RT* of the reaction rate coefficient *k* of the radiation-induced decomposition of TATB at ambient temperature (circles) and about 26 GPa (squares).

The temperature experiments on TATB were performed to extract the activation energy E_A of this radiation-induced decomposition using the Arrhenius equation

$$k = A \exp(-E_A/RT) \tag{5}$$

or

$$\frac{\partial \ln k}{\partial T} = -\frac{E_A}{RT} \tag{6}$$

According to the transition-state theory, E_A is the energy difference between the transition state and the reactant. The Arrhenius plot for ambient conditions and at about 26 GPa is displayed in Figure 14. The analyses yield an activation energy at ambient condition of $E_A = 16(3)$ kJ/mol and at about 26 GPa of 10(3) kJ/mol. These values have a similar order of magnitude as a recent study on the radiation-induced decomposition of SnO ($E_A = 25(7)$ kJ/mol), which also used synchrotron radiation.[32]

Conclusion

We continued our studies of energetic materials subjected to extreme conditions of pressure and ionizing flux and expanded our measurements into the realm of high temperature. The importance of these studies lies in ascertaining the behavior of explosives subjected to a variety of real-world situations involving highly ionizing radiation which include detection and detonation and/or neutralization of explosives and nuclear conditions, including "dirty" bombs. Thus far, we have seen no evidence of global macroscopic heating of the sample and thus may have a unique way to study decomposition of explosives via bond rearrangements on a much slower time scale than shock wave measurements and without macroscopic global heating to obscure the data. The hope is to gain insight into the mechanisms of detonation at the molecular level by learning about decomposition. We also demonstrated a novel experimental technique to study chemistry using synchrotron radiation.

Finally, we also verified that the decomposition rate of PETN scarcely varies with pressure, whereas the decomposition rate of TATB greatly slows with pressure. Thus, we have a unique method to acquire data on such organic materials and/or unstable materials such as TATB that decompose rapidly in the presence of a synchrotron beam by pressurizing them.

Acknowledgment. We are grateful to the HPCAT staff for their technical assistance, particularly Drs. Hanns-Peter Liermann, Wenge Yang, and Yang Ding. We thank Dr. David S. Moore of LANL for supplying us with the submicrometer PETN and TATB samples. We also wish to thank Ed Romano, Brian Yulga, Elizabeth A. Tanis, and Jonathan Larson for helping us with the measurements and Patrick Sims for assistance with the data evaluation. This work was supported by the ARL/UNLV Soldier FERST Cooperative Agreement. Use of the Advanced Photon Source was supported by the U.S. Department of Energy, Office of Science, Office of Basic Energy Sciences, under Contract No. DE-AC02-06CH11357. We gratefully acknowledge support from the U.S. Department of Energy Cooperative Agreement No. DE-FC08-01NV14049 with the University of Nevada Las Vegas and support from the U.S. Army via RDECOM ACQ CTR Contract W9011NF-05-1-0266 and the DOE DE-FC8806NA27684 Cooperative Agreements with UNLV. One of us (M.P.) wishes to acknowledge partial support for this work from the UNLV Institute for Security Studies Summer Research Award and the Nevada/NASA Space Grant program.

References and Notes

(1) Satija, S. K.; Swanson, B.; Eckert, J.; Goldstone, J. A. *J. Phys. Chem*. **1991**, *95*, 10103−10109.

(2) Schettino, V.; Bini, R.; Ceppatelli, M.; Ciabini, L.; Citroni, M. *Adv. Chem. Phys*. **2005**, *131*, 105−242 and references therein.

(3) Baer, B. J.; Oxley, J.; Nicol, M. *High Press. Res.* **1990**, *2*, 99.

(4) Fabbiani, F. P. A.; Pulham, C. R. *Chem. Soc. Rev*. **2006**, *35*, 932−942.

(5) Piermarini, G. J.; Block, S.; Miller, P. J. *J. Phys. Chem*. **1987**, *91*, 3872−3878.

(6) Yoo, C.-S.; Cynn, H. *J. Chem. Phys.* **1999**, *111*, 10229.

(7) Fennelly, A. J.; Woosley, J. K.; McMahon, D. M. *SPIE Proc. X-ray Det. Phys. Appl.* **1993**, *1736*, 159−170.

(8) Hussein, E. M. A. *SPIE Proc. Int. Soc. Opt. Eng*. **1993**, *1736*, 130.

(9) Fondeur, F. F.; Wilmarth, W. R.; Peters, T. B.; Fink, S. D. *Nucl. Technol.* **2005**, *151*, 297.

(10) Walker, D. D., et al. *Sep. Sci. Technol.* **2005**, *40*, 297−309.

(11) Sharma, J.; Beard, B. C. *Nav. Surf. War. Cent. Rep.* NAVSWC TR **1991**, 91−682.

(12) Stolovy, A.; Namenson, A. I.; Aviles, J. B., Jr.; Jones, E. C.; Kidd, J. M. *J. Energy Mater*. **1987**, *5*, 181−238.

(13) Stolovy, A.; Kidd, J. M. *Nav. Res Lab. Memorandum Rep.* **1989**, 6558.

(14) Stolovy, A.; Jones, E. C., Jr.; Aviles, J. B., Jr.; Namenson, A. I.; Fraser, W. A. *J. Chem. Phys.* **1983**, *78*, 229.

(15) Bowden, F. P.; Singh, K. *Proc. Royal Soc. London* Series A, **1954**, Vol. 227, No. 1168; pp 22−37.

(16) Groocock, J. M. *Proc. R. Soc. London A* **1958**, *246* (1245), 225−232.

(17) Aleshov, A. N., et al. *Fiz. Goreniya Vzryva* **2001**, *37* (5), 104−113.

(18) Williams, D. L., et al. *J. Phys. Chem. A* **2003**, *107*, 9491−9494.

(19) Beard, B. C. *Propel. Exp. Pyrotec*. **1991**, *16*, 81−87.

(20) Sharma, J.; Garrrett, W. L.; Owens, F. J.; Vogel, V. L. *J. Phys. Chem*. **1982**, *86*, 1657−1661.

(21) Pravica, M., et al. *J. Phys. Chem. Solids* **2006**, *67*, 2072−2076.

(22) Lipinska-Kalita, K.; Pravica, M. G.; Nicol, M. *J. Phys. Chem. B* **2005**, *109* (41), 19223.

(23) Pravica, M.; Yulga, B.; Liu, Z.; Tschauner, O. *Phys. Rev. B* **2007**, *76*, 064102.

(24) Tschauner, O.; Kiefer, B.; Lee, Y.; Pravica, M.; Nicol, M.; Kim, E. *J. Chem. Phys.* **2007**, *127* (9), 094502.

(25) Pravica, M.; Quine, Z.; Romano, E.; Bajar, S.; Yulga, B.; Yang, W.; Hooks, D. *APS SCCM Conf. Proc*. **2007**, CP955.

(26) Giefers, H.; Pravica, M.; Liermann, H.-P.; Yang, W. *Chem. Phys. Lett*. **2006**, *429*, 304−309.

(27) Rogers, R. N.; Janney, J. L.; Ebinger, M. H. *Thermochim. Acta* **1982**, *59*, 287−298.

(28) Jayaraman, A. *Rev. Mod. Phys*. **1983**, *55* (1), 65−108.

(29) Mao, H. K.; Xu, J.; Bell, P. M. *J. Geophys. Res*. **1986**, *91*, 4673.

(30) Hancock, J. D.; Sharp, J. H. *J. Am. Ceram. Soc.* **1972**, *55*, 74.

(31) Sharp, J. H.; Brindley, G. W.; Narahari Achar, B. N. *J. Am Ceram. Soc.* **1966**, *49*, 379 and references therein.

(32) Giefers, H.; Porsch, F.; Wortmann, G. *Solid State Ionics* **2005**, *176*, 1327−1332.